Accepted Manuscript

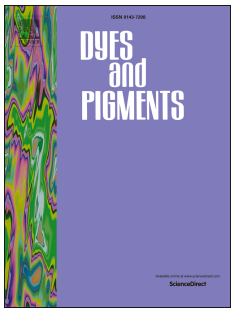

Synthesis and dyeing properties of indophenine dyes for polyester fabrics

Hua Jiang, Qian Hu, Jinfang Cai, Zhihua Cui, Jinhuan Zheng, Weiguo Chen

PII: S0143-7208(18)32546-4

DOI: https://doi.org/10.1016/j.dyepig.2019.03.025

Reference: DYPI 7414

To appear in: *Dyes and Pigments*

Received Date: 19 November 2018

Revised Date: 17 January 2019

Accepted Date: 12 March 2019

Please cite this article as: Jiang H, Hu Q, Cai J, Cui Z, Zheng J, Chen W, Synthesis and dyeing properties of indophenine dyes for polyester fabrics, *Dyes and Pigments* (2019), doi: https://doi.org/10.1016/j.dyepig.2019.03.025.

Synthesis and dyeing properties of indophenine dyes for polyester fabrics

Hua Jiang[a, b], Qian Hu[a], Jinfang Cai[a], Zhihua Cui[a, b, *], Jinhuan Zheng[a, b], Weiguo Chen[a, b, *]

[a] Engineering Research Center for Eco-Dyeing and Finishing of Textiles, Ministry of Education, Zhejiang Sci-Tech University, Hangzhou, 310018, China

[b] Key Laboratory of Advanced Textile Materials and Manufacturing Technology, Ministry of Education of China, Hangzhou 310018, China

* Corresponding author.

E-mail address: zhhcui@zstu.edu.cn (Z. Cui); wgchen_62@126.com (W. Chen).

Abstract: In this study, a series of indophenine dyes (**D1**-**D6**) that show high molecular planarity, were synthesized and applied as dyeing materials for poly(ethylene terephthalate) fabrics. The relationship between the dye molecular structure and dyeing properties, such as dyeing rate and color fastness properties, was investigated. Compared with conventional azo or anthraquinone dyes, the indophenine dyes had a much lower dyeing rate but very good anti-thermomigration properties. This phenomenon indicated that there exists much larger intermolecular interaction between indophenine dye molecules, which was also confirmed by the results of quantum chemical density functional theory (DFT) calculations. The substituent effect of alkyl groups and halogen atoms (F and Cl) was also investigated. The steric hindrance of linked ethyl groups could efficiently promote dyeing performance, while halogen atoms lowered the color acquisition. As a result, **D4** with only two *N*-ethyl groups incorporated on the indophenine backbone showed the best overall dyeing performance.

Keywords: Indophenine; Quinoidal structure; Disperse dye; Dyeing property; Interaction energy; DFT calculation.

1. Introduction

With the polyester industry flourishing, the demand for a variety of high-performance disperse dyes is increasingly sought. In finishing procedures, when dyed polyester fabrics are treated at temperatures higher than 130 ºC (e.g., heat setting or baking with resin), disperse dyes inside the fiber can migrate to the surface, resulting in poor washing and rubbing fastness, especially in the case of deeply dyed fabrics. In addition, when dyeing and finishing polyester/spandex or polyester/viscose blend fabrics, heavy staining occurs on spandex or viscose fibers [1, 2], causing serious color fastness problems.

In the past decades, many efforts have been devoted to develop improved high-fastness disperse dyes [3-11]. One feasible strategy is to develop disperse dyes with increased molecular size, including preparation of disazo disperse dyes [3, 4], introduction of bulkier groups into dye molecules [5], tethering two dye molecules with diester/diurethane groups [6, 7], and polymerizing dyes [8]. However, large dye molecules are more suitable for dyeing polyurethane (PU) fibers than poly(ethylene terephthalate) (PET) fibers, since the free volume in the soft region of a PET fiber is smaller than that of a PU fiber, making it difficult for large dye molecules to penetrate the PET fiber. Recently, Wang et al. demonstrated that introduction of a planar ring moiety (e.g., phthalimide or benzodifuranone) into the dye molecule is an effective approach to restrain the thermal migration of dye molecules [12-14]. The increased molecular coplanarity brings about a larger intermolecular interaction energy, which increases the dye-dye and dye-fiber forces, leading to better fastness properties.

In our efforts to search for new chromophores for designing high-performance disperse dyes, we noticed that there emerged thiophene-based quinoidal compounds used in the field of opto-electronic materials [15, 16]. In particular, quinoidal thiophene derivatives display very high rigidity and

planarity owing to the double bond present between each cyclic unit. Such molecular planarity is useful for enhancing dye-dye and dye-fiber interactions, favoring better fastness [13]. Furthermore, quinoidal molecules usually exhibit low energy bandgaps with very large molar extinction coefficients [17, 18]. Therefore, it is promising to apply quinoidal thiophene as a chromophore into textile dyestuffs. Very recently, we reported the structure-property relationships of quinoidal bithiophene dyes that were end-capped with cyano or ester groups for dyeing PET fabric [19]. As expected, the high planarity of these dyes produced excellent washing, rubbing, and sublimation fastness. The challenge of forming single dye molecules in the dyeing process was overcome by introduction of suitable alkyl groups into the quinoidal backbone. Hence, quinoidal thiophene derivatives were demonstrated as potential disperse dyes.

Indophenine, a well-known blue dyestuff based on the quinoidal bithiophene backbone, can be readily synthesized by isatin and thiophene in the presence of concentrated sulfuric acid [20]. A remarkable color change occurs, termed the “indophenine reaction”, which has mainly been used as a visual colorimetric indicator of trace amounts of thiophene. However, because of its poor solubility originated from strong π-π interaction, the direct application of indophenine was very limited. Recently, indophenine derivatives with long alkyl chains (up to 12 carbons) were designed and synthesized, resulting in good solubility in common organic solvents, and subsequent use as semiconductor materials [21, 22]. On the other hand, indophenine derivatives with short alkyl chains remain poor solubility [20], and their properties and application have not been fully explored.

In this study, we devised a PET dyeing method using six readily synthesized indophenine derivatives as disperse dyes. There are three reasons for this molecular design. (i) The larger quinoidal backbone of the indophenine molecule enhances the dye-dye and dye-fiber forces, which

provides better fastness on dyed fabrics, especially related to anti-thermomigration. (ii) The nitrogen of the indolin-2-one moiety in the indophenine molecule provides a convenient site to introduce an alkyl chain. Thus, fine-tuning intermolecular interactions becomes possible for facilitating the dyeing process, as we previously reported [19]. (iii) The synthesis of indophenine dyes is quite facile and scale-up is feasible, which favors disperse dye development for industrial dyeing applications. Although indophenine is reported to have six *cis-trans* isomers [22], no discernable evidence of decreased dyeing performance has been attributed to the coexistence of these isomers. Actually, our dyeing experiments with derivatized indophenine dyes produced bright blue shades on PET fabrics with excellent wet fastness. *N*-ethyl groups were found to promote the dyeing performance, while halogens (i.e., F and Cl atoms) decreased color acquisition. To gain greater insight into structure-property relationships of derivatized indophenine dyes, the effect of quinoidal planarity on dyeing performance and the halogen atom effect have also been studied by calculating the intermolecular interaction energy.

2. Experimental section

2.1 Materials and instruments

Unless otherwise specified, all chemicals and solvents were purchased commercially (Adamas Reagent Co., Ltd.). Two commercial dyes (**D7**, C.I. disperse blue 291; **D8**, C.I. disperse blue 56) were provided by Jihua Jiangdong Chemical Co., Ltd. These two dyes had been purified by column chromatography before use. All reactions were carried out in dried glassware and nitrogen atmosphere. Solvents were previously dried by conventional methods and stored under nitrogen. Air- and water-sensitive solutions were transferred with hypodermic syringes.

NMR spectra were recorded with a Bruker DMX 400 MHz NMR spectrometer at room

temperature in $CDCl_3$ or DMSO-d_6. Electrospray ionization mass spectra (ESI-MS) were recorded on a Thermo Lcq Fleet mass spectrometer in a scan range of 200–2000 amu. Accurate mass data were obtained by high resolution mass spectrometry performed on a solanX 70 FT-MS spectrometer. Infrared (IR) spectra (4000-400 cm^{-1}) were recorded using a Nicolet FT-IR 170X spectrophotometer on KBr disks. Melting points were measured on Mettler-Toledo melting point apparatus and were uncorrected. UV-Vis spectra were recorded with a Shimadzu UV-2600 double-beam spectrophotometer using a quartz glass cell with a path length of 1.0 cm. Dyeing of polyester fabrics was operated by using DYE-24 adjustable dyeing machine (ShangHai Chain-Lih, China). The color yield of the dyed fabrics was measured by Datacolor SF 600X spectrophotometer (Datacolor, Switzerland).

2.2 Preparation of indophenine dyes

*2.2.1 3,3'-([2,2'-Bithiophenylidene]-5,5'-diylidene)bis(indolin-2-one) (**D1**)*

Concentrated sulfuric acid (15 mL) was added to a solution of isatin (20 mmol, 2.95 g) and thiophene (44 mmol, 3.70 g) in toluene (40 mL) at 0 ºC. It was found that all colored solutes were involved into sulfuric acid layer, and the color became dark blue. The mixture continued to react at 0 ºC for 3 h. After the reaction was completed, transparent toluene solvent was removed and the residue was poured into icy water (100 mL) carefully. The crude product was obtained by filtration, followed by washing with an excess of water, ethanol, hexane and dichloromethane successively, until each liquid became clear. Finally, a drying process in vacuum gave the target compound as a dark blue solid, 3.52 g, 82%. Mp: >350 ºC. ESI-MS (100%, negative) m/z = 425 ($[M-H]^-$); ESI-HRMS (m/z) Calcd. for $C_{24}H_{14}N_2O_2S_2$: 426.0497 ($[M]^+$), found: 426.0497; IR (KBr) ν = 1676 cm^{-1} (C=O).

*2.2.2 3,3'-([2,2'-Bithiophenylidene]-5,5'-diylidene)bis(5-fluoroindolin-2-one) (**D2**)*

The same procedure as in 2.2.1 was used, except that 5-fluoroindoline-2,3-dione (20 mmol) was used as starting material. Dark blue solid, 3.30 g, 71%. Mp: >350 ºC. ESI-MS (100%, negative) *m*/*z* = 461 ([M-H]$^-$); ESI-HRMS (*m*/*z*) Calcd. for $C_{24}H_{12}F_2N_2O_2S_2$: 462.0308 ([M]$^+$), found: 462.0312; IR (KBr) ν = 1685 cm^{-1} (C=O).

*2.2.3 3,3'-([2,2'-Bithiophenylidene]-5,5'-diylidene)bis(5-chloroindolin-2-one) (**D3**)*

The same procedure as in 2.2.1 was used, except that 5-chloroindoline-2,3-dione (20 mmol) was used as starting material. Dark blue solid, 2.96 g, 59%. Mp: >350 ºC. ESI-MS (100%, negative) *m*/*z* = 493 ([M-H]$^-$); ESI-HRMS (*m*/*z*) Calcd. for $C_{24}H_{12}Cl_2N_2O_2S_2$: 516.9609 ([M+Na]$^+$), found: 516.9628; IR (KBr) ν = 1681 cm^{-1} (C=O).

*2.2.4 1-Ethylindoline-2,3-dione (**4**)*

A solution of sodium hydride (22 mmol, 0.88 g, 60% wt) in anhydrous DMF (30 mL) was added to a solution of isatin (20 mmol, 2.94 g) in anhydrous DMF (20 mL) at 0 ºC under nitrogen atmosphere. The solution became dark purple. After stirring for 30 min, iodoethane (21 mmol, 3.28 g) was added, and the reaction mixture was stirred for another 5 h at room temperature. Water was added to quench the reaction and it was extracted with dichloromethane. The organic layer was washed with water and dried over anhydrous magnesium sulphate. The crude product was purified by column chromatography (petroleum ether:CH_2Cl_2 = 1:1) to afford compound **4** as orange solid [23]. 2.62 g, 75%. Mp: 88-89 ºC. ^{1}H NMR (400 MHz, $CDCl_3$) δ 7.60–7.56 (m, 2H), 7.10 (t, *J* = 7.6 Hz, 1H), 6.90 (d, *J* = 8.2 Hz, 1H), 3.77 (q, *J* = 7.2 Hz, 2H), 1.30 (t, *J* = 7.6 Hz, 3H). ^{13}C NMR (100 MHz, $CDCl_3$) 183.18, 157.28, 150.08, 138.08, 124.61, 123.08, 116.90, 109.79, 34.40, 11.98; IR (KBr) ν = 1739 (C=O), 1610 cm^{-1} (C=O).

*2.2.5 3,3'-([2,2'-Bithiophenylidene]-5,5'-diylidene)bis(1-ethylindolin-2-one) (**D4**)*

The same procedure as in 2.2.1 was used, except that 1-ethylindoline-2,3-dione (10 mmol) was used as starting material. Dark blue solid, 1.18 g, 49%. Mp: 252-254 ºC. ESI-MS (100%, negative) *m*/*z* = 482 ($[M]^-$); ESI-HRMS (*m*/*z*) Calcd. for $C_{28}H_{22}N_2O_2S_2$: 482.1123 ($[M]^+$), found: 482.1132; IR (KBr) ν = 1681 cm^{-1} (C=O).

*2.2.6 1-Ethyl-5-fluoroindoline-2,3-dione (**5**)*

The same procedure as in 2.2.4 was used, except that 5-fluoroindoline-2,3-dione (20 mmol) was used as starting material. Orange red solid, 3.08 g, 80%. Mp: 126-128 ºC. ^{1}H NMR (400 MHz, $CDCl_3$) δ 7.33-7.28 (m, 2H), 6.87 (dd, J^1 = 9.2 Hz, J^2 = 3.6 Hz, 1H), 3.78 (q, *J* = 7.2 Hz, 2H), 1.31 (t, *J* = 7.2 Hz, 3H). ^{13}C NMR (100 MHz, $CDCl_3$) δ 182.90, 160.12, 157.51 (d, *J* = 33.4 Hz), 146.49, 124.48 (d, *J* = 24.0 Hz), 117.85 (d, J = 6.9 Hz), 111.96 (d, *J* = 24.0 Hz), 111.22 (d, *J* = 7.1 Hz), 34.80, 12.09; IR (KBr) ν = 1735 (C=O), 1618 cm^{-1} (C=O).

*2.2.7 3,3'-([2,2'-Bithiophenylidene]-5,5'-diylidene)bis(1-ethyl-5-fluoroindolin-2-one) (**D5**)*

The same procedure as in 2.2.1 was used, except that 1-ethyl-5-fluoroindoline-2,3-dione (10 mmol) was used as starting material. Dark blue solid, 0.89 g, 34%. Mp: decomposition before melting. ESI-MS (100%, negative) *m*/*z* = 518 ($[M]^-$); ESI-HRMS (*m*/*z*) Calcd. for $C_{28}H_{20}F_2N_2O_2S_2$: 518.0934 ($[M]^+$), found: 518.0943; IR (KBr) ν = 1676 cm^{-1} (C=O).

*2.2.8 5-Chloro-1-ethylindoline-2,3-dione (**6**)*

The same procedure as in 2.2.4 was used, except that 5-chloroindoline-2,3-dione (20 mmol) was used as starting material [24]. Orange red solid, 3.23 g, 77%. Mp: 130-132 ºC. ^{1}H NMR (400 MHz, $CDCl_3$) δ 7.56-7.53 (m, 2H), 6.87 (dd, J^1 = 4.8 Hz, J^2 = 4.0 Hz, 1H), 3.78 (q, *J* = 7.2 Hz, 2H), 1.30 (t, *J* = 7.2 Hz, 3H). ^{13}C NMR (100 MHz, $CDCl_3$) δ 182.45, 157.05, 148.70, 137.52, 129.02, 124.84,

118.09, 111.34, 34.89, 12.16; IR (KBr) ν = 1735 (C=O), 1608 cm^{-1} (C=O).

*2.2.9 3,3'-([2,2'-Bithiophenylidene]-5,5'-diylidene)bis(5-chloro-1-ethylindolin-2-one) (**D6**)*

The same procedure as in 2.2.1 was used, except that 5-chloro-1-ethylindoline-2,3-dione (10 mmol) was used as starting material. Dark blue solid, 1.06 g, 38%. Mp: >350 ºC. ESI-MS (100%, negative) *m*/*z* = 550 ($[M]^-$); ESI-HRMS (*m*/*z*) Calcd. for $C_{28}H_{20}Cl_2N_2O_2S_2$: 550.0343 ($[M]^+$), found: 550.0335; IR (KBr) ν = 1678 cm^{-1} (C=O).

2.3 Dyeing procedure

Dye dispersion solution was prepared by grinding the mixture of indophenine dye (0.5 g), dispersant NNO (Naphthalenesulfonic acid/formaldehyde condensation product, 1.0 g), Zirconium beads (Φ 0.2 mm, 50 g) and water (50 mL) in a laboratory miniature quartz tube equipped with mechanical stirrer. After the average particle size decreased to lower than 500 nm checked by laser particle size analyzer (zetasizer Nano S, UK), the mixture was filtered into volumetric flask. Then, a solution with certain concentration was prepared after additional water was added.

The polyester fabric (PET 100%, 188 dtex, 2/2 twill) was dyed with dye amount of 1.0% owf (weight of dye to fabric), kept at a liquor ratio of 1:50 and pH at 5.0 (using acetic acid). The dyeing temperature started at 30 °C, then raised to 130 °C with heating rate of 2.0 °C/min and maintained at 130 °C for 1 h. After cooling, the dyed fabric was picked out and treated with a solution of sodium dithionite (2 g/L) and sodium hydroxide (2 g/L) at 80 °C for 5 min. Finally, the fabric was rinsed with clean water and dried at 60 °C.

2.4 Color assessment

Color depths of dyed PET fabrics were obtained from dyed samples at maximum absorption wavelength. Each sample was measured three times in a different area and an average value was used.

The "*K/S*" value was calculated based on the Kubelka-Munk equation:

$$K/S = \frac{(1-R)^2}{2R}$$

where *K* is the adsorption coefficient, *S* is the scattering coefficient, and *R* is the reflectance of the dyed sample.

In the study of dyeing rate curve, the color intensity (%) was calculated as follows [13]:

$$\text{Color intensity (\%)} = \frac{\text{Color depth}_{\text{batch sample}}}{\text{Color depth}_{\text{standard sample}}}$$

$$\text{Color depth} = \int_{400\text{ nm}}^{700\text{ nm}} f(x)_{K/S}\mathrm{d}x$$

The color coordinates of indophenine dyes were determined on CE-7000A Gretag-Macbeth computer color matching system. The color values were expressed by using CIE 1976 Color Space method. The coordinates used to determine color values are "*L**" for lightness, "*a**" for redness (positive value) and greenness (negative value), "*b**" for yellowness (positive value) and blueness (negative value), "*C**" for chroma and "*h*°" for hue angle.

2.5 Measurement of migration degree

A piece of dyed PET fabric (sample A) at 1% owf color shade was sewed with another piece of un-dyed PET fabric (sample B) having equal weight. The combined fabrics were put into a dyeing bath (liquor ratio 1:30, pH 5.0), then heated from 30 °C to 130 °C with heating rate of 2.0 °C/min and maintained at 130 °C for 1 h. After cooling, the two samples were picked up and dried. The migration degree (%) was calculated as follows:

$$\text{Migration degree (\%)} = \frac{(K/S)_{\mathrm{B}}}{(K/S)_{\mathrm{A}}} \times 100$$

where $(K/S)_{\mathrm{A}}$ is the *K*/*S* value of sample A after treatment, $(K/S)_{\mathrm{B}}$ is the *K*/*S* value of sample B after treatment.

2.6 Colorfastness

The color fastnesses to washing, rubbing, sublimation and light were measured in accordance with the ISO 105-C06: 2010 (C1S), ISO 105-X16: 2016, ISO 105-X11: 1994 and ISO 105-B02: 2014, respectively.

2.7 Density functional theory calculation

All theoretical calculations were performed with Gaussian09 programs [13, 25]. Optimized ground state geometry of the lowest energy conformation for **D1**-**D6** were calculated at the B3LYP/6-311G (d, p) level. HOMO/LUMO energy and electron density distribution were calculated at B3LYP/6-311G ++ (d, p) level. Intermolecular interaction energy was computed by DFT/ωB97XD method with 6-311G (d, p) basis set for indophenine dyes **D1**-**D3**. To simplify the calculation, only *trans* isomer (*E*,*E*,*E* isomerization) of indophenine dyes was computed.

3. Results and discussion

3.1 Synthesis and photophysical properties

The six indophenine dyes were synthesized according to a reported method [20], with the synthetic route shown in **Scheme 1**. Among the derivatives, **D1**, **D2**, and **D3** could easily be obtained by the "indophenine reaction" using isatin, 5-fluoroisatin, or 5-chloroisatin as starting materials, respectively. For **D4**-**D6**, ethyl groups were firstly introduced by *N*-alkylation (of isatin, 5-fluoroisatin, or 5-chloroisatin) to give *N*-ethyl isatin derivatives, which subsequently underwent the "indophenine reaction" to afford the desired products smoothly (**D4**, **D5**, and **D6**, respectively). As expected, all six dyes exhibited very poor solubility in common organic solvents (e.g., chloroform, toluene, and tetrahydrofuran). Thus, we purified the synthesized dyes by washing with plenty of water, ethanol, hexane, and dichloromethane to remove residual sulfuric acid, thiophene, and other

possible soluble byproducts. The poor solubility also brought serious complications for structural characterization, in which only mass spectral characterization of the six dyes was possible. Indophenine dyes are reported to have six structural conformations due to *cis-trans* isomerism [22]. Nevertheless, our previous results demonstrated that a mixture of isomers had a negligible effect on dye effectiveness [19]. In addition, the properties of two purified commercial blue disperse dyes, namely C.I. disperse blue 291 (**D7**) and C.I. disperse blue 56 (**D8**; **Fig. 1**), are also presented here for comparison.

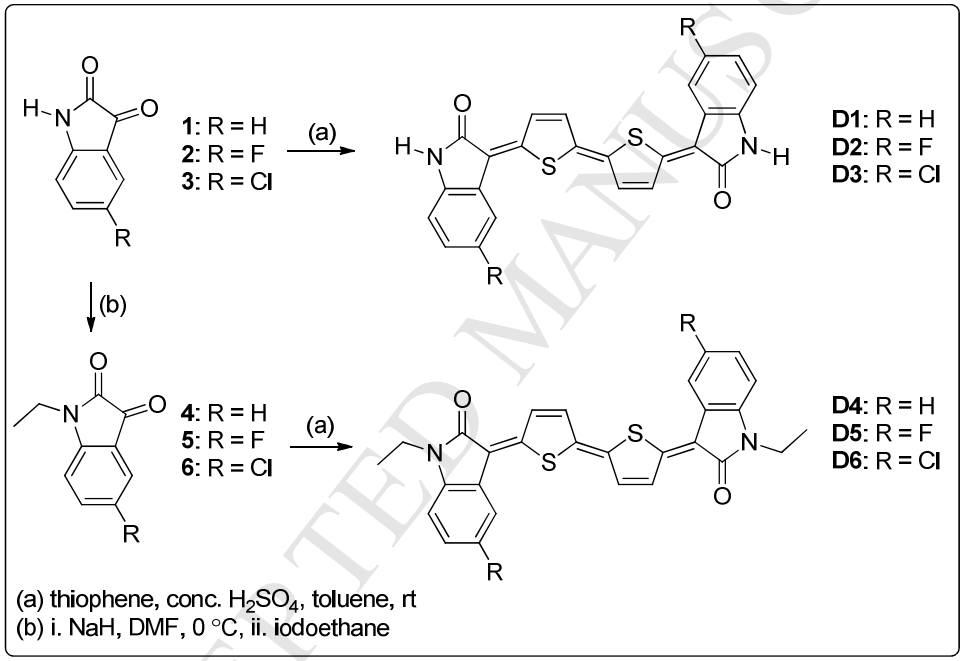

Scheme 1. Molecular structures and synthetic route for indophenine dyes **D1**-**D6**.

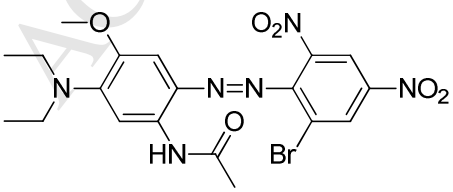

D7 (C.I. disperse blue 291)

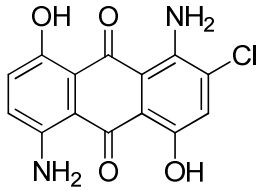

D8 (C.I. disperse blue 56)

Fig. 1. Structures of two commercially available blue disperse dyes.

The UV-vis absorption spectra of both indophenine dyes and commercial dyes were measured in order to understand their optical properties. Thanks to their moderate solubility in DMF, dilute absorption spectra of indophenine dyes could be recorded, as shown in **Fig. 2**. All the quinoidal molecules **D1-D6** exhibited broad absorption bands from 400 nm to 800 nm with λ_{max} of approximately 631 nm to 642 nm, similar to conventional dyes **D7** and **D8**. The maximum absorption wavelengths of indophenine dyes **D1-D3** were slightly red-shifted compared with **D4-D6**, while the latter showed higher extinction coefficients.

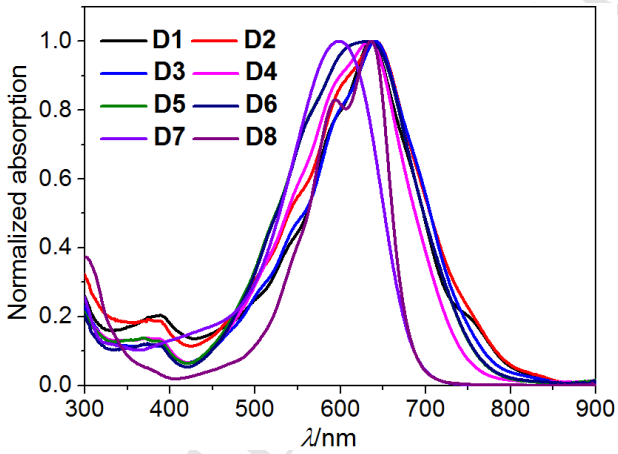

Fig. 2. UV-vis spectra of indophenine dyes **D1-D8** in DMF.

Table 1. UV-vis absorption data of dyes **D1-D8** in DMF.

	D1	**D2**	**D3**	**D4**	**D5**	**D6**	**D7**	**D8**
λ_{max}/nm	636	640	642	633	631	632	598	636
ε/L·mol^{-1}cm^{-1}	26434	23303	33095	39021	40497	52665	39048	18509
$\Delta\nu_{1/2}$/nm [a]	141	171	151	150	173	172	123	100

[a] half-band width.

3.2 Dyeing properties

3.2.1 Color assessment

The synthesized indophenine dyes were applied to PET fabrics at 1.0% owf color shade by using the high temperature exhaustion dyeing method at 130 ºC [19]. The dye exhaustion and color parameters of dyed PET fabrics are summarized in **Table 2**. Our initial dyeing attempt of polyester fabrics resulted in blue shades with excellent color uniformity (**Fig. 3**). It can be seen that the six indophenine dyes exhibited large differences in their dyeing performance in terms of dye exhaustion and color depth. Among them, **D4** showed acceptable dye exhaustion and color depth, indicating the positive effect of *N*-ethyl groups. The introduction of halogen atoms (**D2**, **D3**, **D5** and **D6**) was found to give a negative influence on the overall dyeing performance. The low exhaustion and precipitation of some dye particles at the bottom of the bath after dyeing suggest difficulty in formation of single indophenine dye molecules, indicating the existence of large dye-dye interactions.

Table 2. Dye exhaustion and color parameters of dyed PET fabrics for dyes **D1**-**D8**.

	Exhaustion/%	λ_{max}/nm [a]	*K*/*S*	*L**	*a**	*b**	*C**	*h*º
D1	74.4	650	11.7	34.81	-0.84	-25.89	25.91	268.15
D2	61.6	650	7.8	37.28	1.19	-23.64	23.67	272.87
D3	54.2	650	8.8	34.76	2.58	-22.73	22.87	276.28
D4	85.0	650	17.7	30.13	6.89	-33.11	33.82	281.76
D5	44.3	650	9.8	35.03	5.99	-34.06	34.58	279.98
D6	55.6	650	4.8	44.41	2.77	-29.00	29.13	275.46
D7	97.7	610	19.5	23.08	-1.91	-21.65	21.73	264.95
D8	93.3	630	20.3	28.94	8.01	-39.66	40.46	281.41

[a] Data collected from *K*/*S* curves.

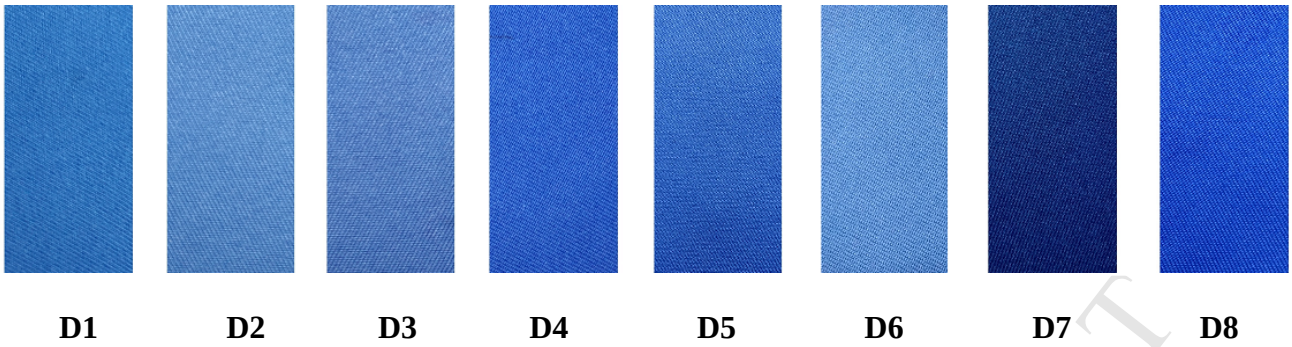

Fig. 3. Digital photos of the dyed PET fabrics under D_{65} illuminant.

3.2.2 Dyeing rate curve

As shown in **Fig. 4**, the dyeing rate curves for indophenine dyes **D1-D6** as well as commercial dyes **D7-D8** are depicted by collecting *K*/*S* data every 10 min during the dyeing process. It emerged that the indophenine dyes **D1-D6** started dyeing at 100–110 ºC, but most of them needed much more time than **D7** and **D8** to reach dyeing equilibrium. The dyeing rate of synthesized indophenine dyes was much lower than that of conventional azo or anthraquinone dyes. This suggests that there are much larger dye-dye interactions between indophenine dye molecules and more energy necessary to weaken the intermolecular forces compared to conventional dyes. Specifically, **D4**, with two *N*-ethyl groups, reduced the dye-dye interactions such that it exhibited a comparable dyeing rate to **D7**. Halogen atom substituted dyes (such as **D3**, **D5**, and **D6**) showed much lower dyeing rates. This suggests that halogen atoms provide larger intermolecular interactions.

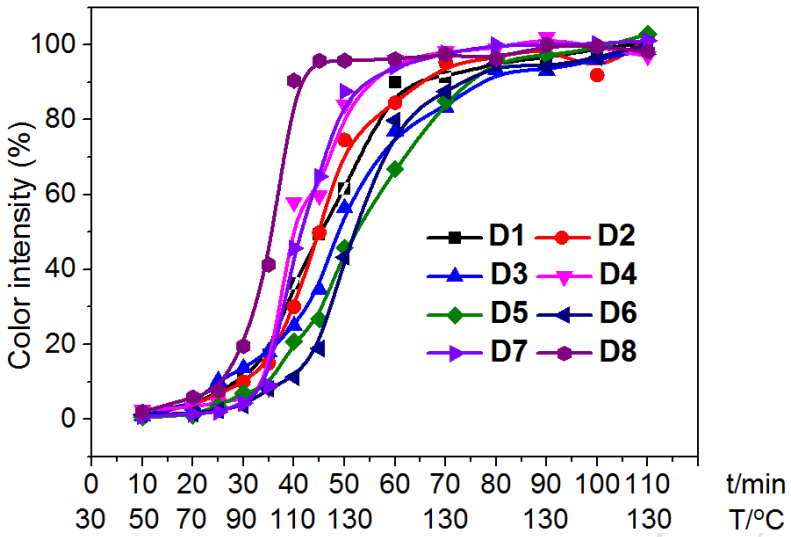

Fig. 4. Dyeing rate curves for indophenine dyes **D1-D6** and commercial dyes **D7-D8**.

3.2.3 Effect of dyeing temperature

We examined the effect of dyeing temperature using **D4** (**Fig. 5**). The dyeing procedure was similar to that described in *2.3*, except that the temperatures were set at 125 ºC, 130 ºC, 135 ºC and 138 ºC. The resulting *K/S* values in one batch experiment were 11.4, 16.5, 19.1 and 19.6, respectively. Compared with **D7** and **D8**, it is encouraging that a competitive color depth using indophenine dyes could be obtained at higher temperature. The fact that the *K/S* value increases remarkably with increasing temperature confirmed the prediction of large dye-dye interactions for indophenine dyes.

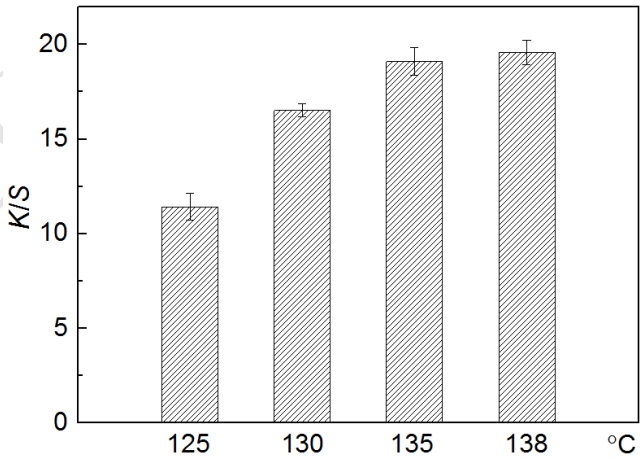

Fig. 5. *K/S* values of PET fabrics dyed with **D4** at different temperatures.

3.2.3 Color fastness

The results of color fastness testing for PET fabrics dyed with indophenine dyes **D1**-**D6** at 1.0% owf color shade are shown in **Table 3**. All these indophenine dyes exhibited excellent washing, rubbing, and sublimation fastness on PET fabrics. It should be noted that the tested samples had undergone a reductive cleaning process with sodium dithionite (2 g/L) and sodium hydroxide (2 g/L) at 80 ºC for 5 min before testing. On one hand, the reducing conditions might convert the quinoidal structure into the colorless aromatic state [15]. On the other hand, amide bonds in indophenine dyes are presumably hydrolyzed to soluble groups. Thus, dyes on the fabric surface could be readily removed and good wet fastness properties were obtained. Because of the good thermal stability at high temperature [16], indophenine dyes showed less color staining of PET or cotton than **D7** or **D8**, as well as better sublimation fastness. We attribute these effects to strong dye-dye and dye-fiber interaction energies, which can prevent the dye from both transferring to an un-dyed fabric and undergoing sublimation upon heating. However, the light fastness of indophenine dyes is generally poor, likely due to their ease of decay to colorless aromatic states under a Xenon light source (see **Fig. S1**) [26].

The anti-thermomigration properties of indophenine dyes on PET fabrics were also investigated. After the dyed PET fabrics (1% owf color shade) were treated with un-dyed fabrics under high temperature and pressure, the degree of migration was calculated and shown in **Fig. 6**. Compared with **D7** and **D8**, the indophenine dyes showed remarkably reduced dye migration properties. This result clearly indicates that larger dye-fiber interactions exist in fabrics dyed with indophenine dyes. F/Cl substituted dyes had relatively lower degrees of migration, again suggesting that F/Cl atoms assist in increasing intermolecular interactions.

Table 3. Fastness properties of dyes **D1-D8** on PET fabrics.

Dye	Wash fastness			Rubbing fastness		Sublimation fastness			Light fastness
	Change	Stain		Dry	Wet	Change	Stain		
		PET	Cotton				PET	Cotton	
D1	5	5	5	5	4-5	5	4-5	5	2
D2	5	5	5	4-5	4-5	5	5	5	3
D3	5	5	5	4-4	4	5	5	5	3
D4	5	5	5	4-5	4	5	4-5	5	2-3
D5	5	5	5	4-5	4-5	5	5	5	3
D6	5	5	5	4	4	5	5	5	2-3
D7	5	5	5	4	4	4-5	4	3-4	6-7
D8	5	5	5	4-5	4	4-5	3-4	3	6-7

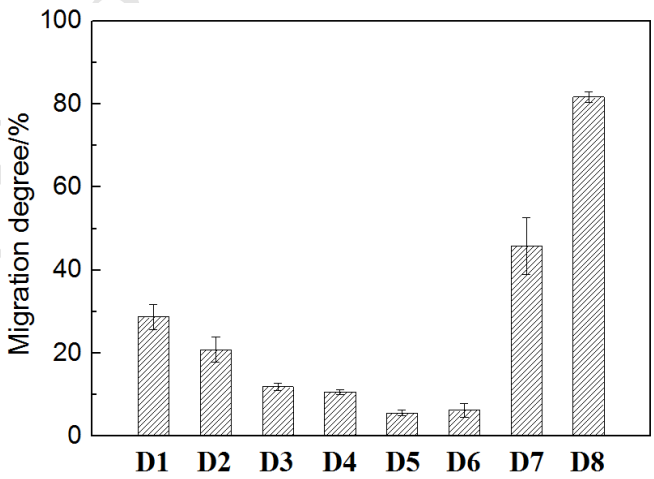

Fig. 6. Migration of dyes **D1-D8** from dyed PET fabrics to un-dyed PET fabrics.

3.3 Quantum chemical calculations

3.3.1 Molecular geometry and energy

To better understand the structure-property relationships of indophenine dyes, density functional theory (DFT) calculations were carried out based on the indophenine backbone. The six indophenine dye molecules were firstly optimized at B3LYP/6-311G (d, p) level. Then, energy information of these dyes was calculated at B3LYP/6-311G++ (d, p) level based on the optimized molecular geometry configuration. The results are shown in **Fig. 7** and summarized in **Table 4**.

Side views of the six molecular geometry configurations intuitively showed a very planar quinoidal backbone; this planarity is the origin of large π-π stacking interactions, which lead to formation of strong dye-dye and dye-fiber forces. For **D4**-**D6**, the *N*-ethyl groups are found above and below the quinoidal plane due to rotation of the C-C single bond. In this case, steric hindrance of *N*-ethyl groups should favor the generation of more single dye molecules by disrupting π-π stacking interactions, as demonstrated in our previous study [19]. For all studied indophenine dyes, both the HOMO (highest occupied molecular orbital) and LUMO (lowest unoccupied molecular orbital) electron cloud densities were evenly distributed across the entire conjugated indophenine backbone, which presumably influences intermolecular electrostatic interactions.

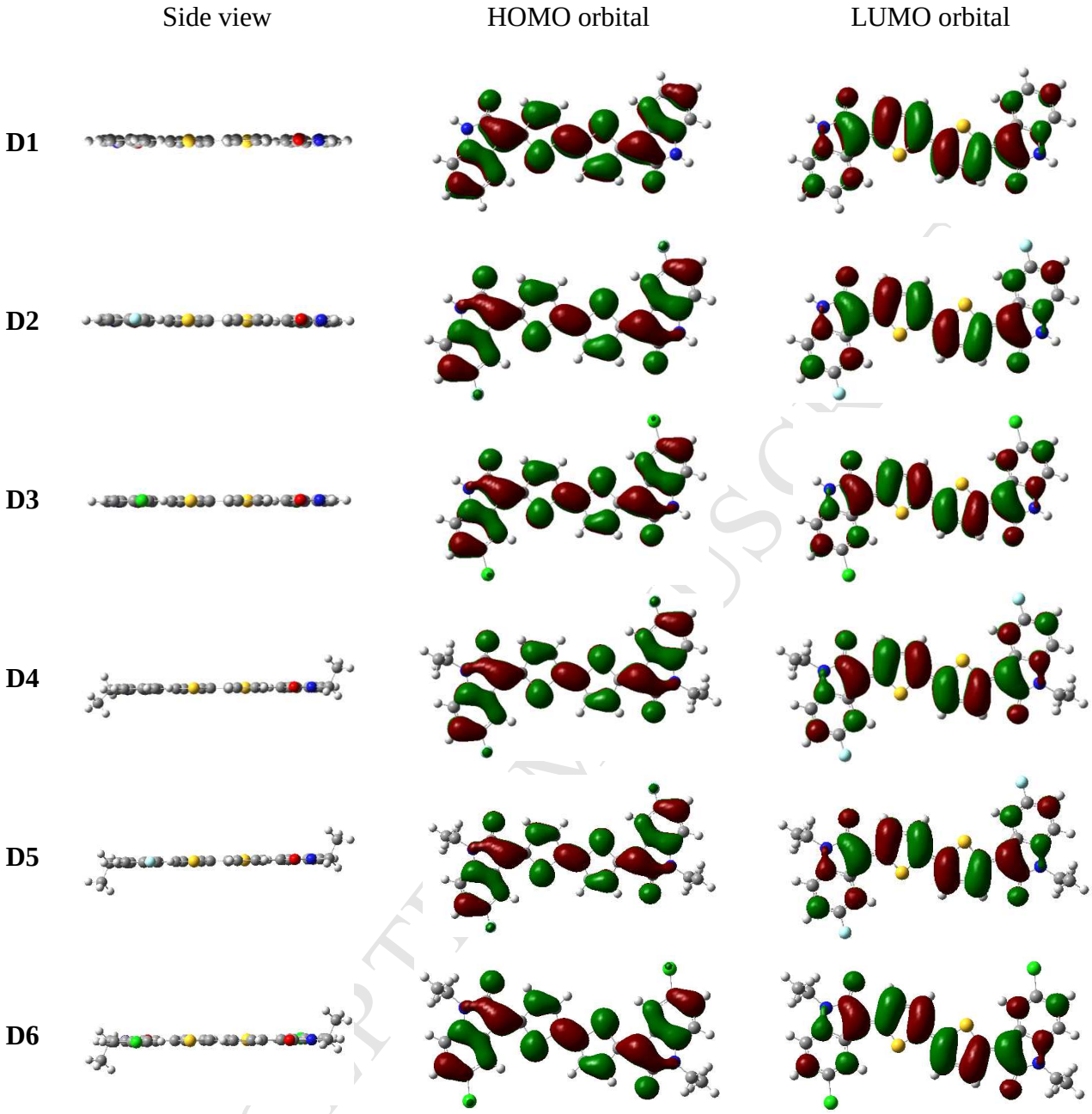

Fig. 7. DFT calculations for optimized molecular geometries and HOMO/LUMO orbital diagrams of **D1-D6**.

Table 4. Energy information of optimized molecular geometry configuration for indophenine dyes.

	E (a.u.)	Dipole moment (Debye)	LUMO (eV)	HOMO (eV)	ΔE (eV)
D1	-1979.67294	0.0001	-3.4287	-5.2948	1.8661
D2	-2178.19876	0.0001	-3.6168	-5.4757	1.8589
D3	-2898.91476	0.0001	-3.6815	-5.5342	1.8527
D4	-2136.97061	0.0055	-3.3773	-5.2428	1.8655
D5	-2335.49527	0.0011	-3.5577	-5.4170	1.8593
D6	-3056.21168	0.0001	-3.6192	-5.4869	1.8677

3.3.2 Interaction energy

The inter-ring interaction from π-π stacking between two dye molecules and the van der Waals' forces between dye molecules and PET fibers were focused on to determine interaction energies. When PET fabrics are dyed with conventional monoazo dyes, benzene-benzene interactions represent both dye-dye and dye-fiber forces. For indophenine dyes, the dye-fiber force is an indophenine-benzene interaction while the dye-dye force is an indophenine-indophenine interaction. As reported by Wang et al., face-to-face configurations are more stable than edge-to-face or point-to-face configurations [12, 13]. Here, face-to-face configurations of indophenine dyes, in which the dashed line indicates the ring overlap center, were modeled (**Fig. 8**). The dimer model **a1** represents the benzene-benzene interaction, **a2-a4** represent the **D1**-benzene interaction, and **a5-a8** indicate possible **D1-D1** interactions.

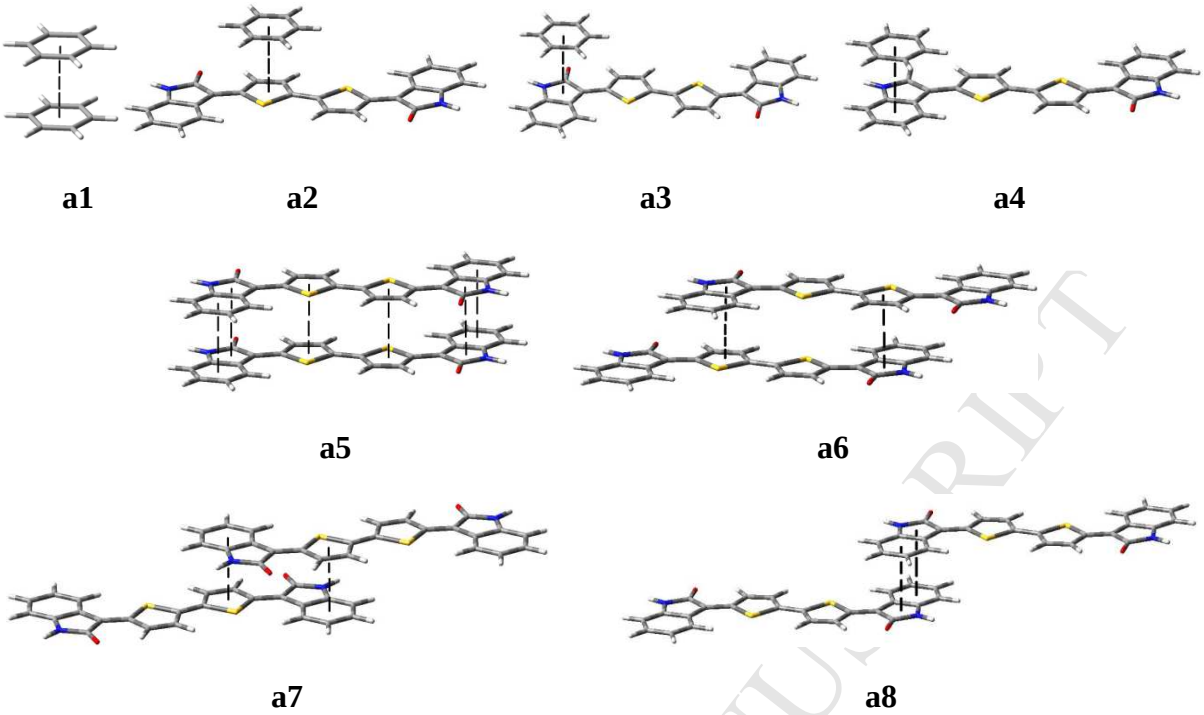

Fig. 8. Molecule interaction energy models for **D1**.

The intermolecular interaction energy was obtained with the DFT/ωB97XD method in 6-311G (d, p) level based on the above dimer model, with the results shown in **Fig. 9**. Both the **D1**-benzene interaction energy and **D1**-**D1** interaction energy initially fell to minimum values at 3.5-3.75 Å, and then slowly increased with increasing inter-ring distance. This suggests that such interaction energies belong to long-range interactions. **D1**-benzene interaction energies for **a2** (-32.57 kJ/mol), **a3** (-33.38 kJ/mol) and **a4** (-22.74 kJ/mol) at 3.5 Å were much larger than the benzene-benzene interaction energy (-10.97 kJ/mol, minimum at 3.75 Å), indicating that a higher interaction energy exists between **D1** and the PET fiber. Interestingly, **a2** and **a3** configurations displayed much larger interaction energies than **a4**, possibly due to favorable electrostatic attractive forces from the presence of electronegative heteroatoms [13]. For the **D1**-**D1** interaction, we constructed the models by translating the indophenine backbone overlap along the quinoidal π-conjugation pathway from **a5**

to **a8**. Among these models, the **a5** configuration, where all atoms completely overlap, showed very strong electrostatic repulsion at close distance (d < 3.5 Å). For the remaining **D1-D1** configurations, **a6** with three groups of interacting rings appears to be the most stable configuration. The lowest interaction energies for **a6**, **a7**, and **a8** at 3.5 Å were -119.89 kJ/mol, -73.35 kJ/mol, and -52.24 kJ/mol, respectively.

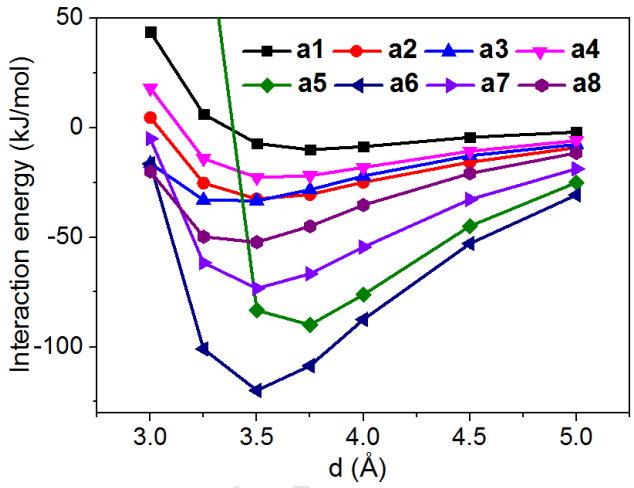

Fig. 9. Benzene-benzene, **D1**-benzene and **D1-D1** interaction energies.

The electrostatic potential energy diagrams for **D1** and **a2-a8** configurations are shown in **Fig. 10**. The total density diagram of **D1** indicates that the most electronegative (O atom) and electropositive (N-H bond) poles are located at the edge of the pyrrol-2-one moiety. The S atoms, quinoidal olefinic bond, and benzene rings remain with very little differences in electronegativity. The Mulliken charges of **D1** (**Fig. S2**) exhibit much larger differences among each atom on the pyrrol-2-one and quinoidal thiophene moieties than those of the benzene moiety. This charge differentiation benefits molecular attraction, thus the **a2** and **a3** configurations exhibit larger interaction energies than the **a4** configuration. The **D1-D1** interaction models of the **a5** configuration clearly showed an entirely

electrostatic repulsive force, which reduced the configuration stability. In comparison, partly overlapped **a6**-**a8** configurations possessed much more electrostatic attractive interaction. Since the dipole moments of the calculated indophenine molecules are close to zero (see **Table 4**), dispersion forces are also believed to have a large effect on the **D1**-**D1** interaction. The larger contact surface in the **a6** configuration therefore provides greater dispersion forces, which contribute to the highest interaction energy among **a6**-**a8**.

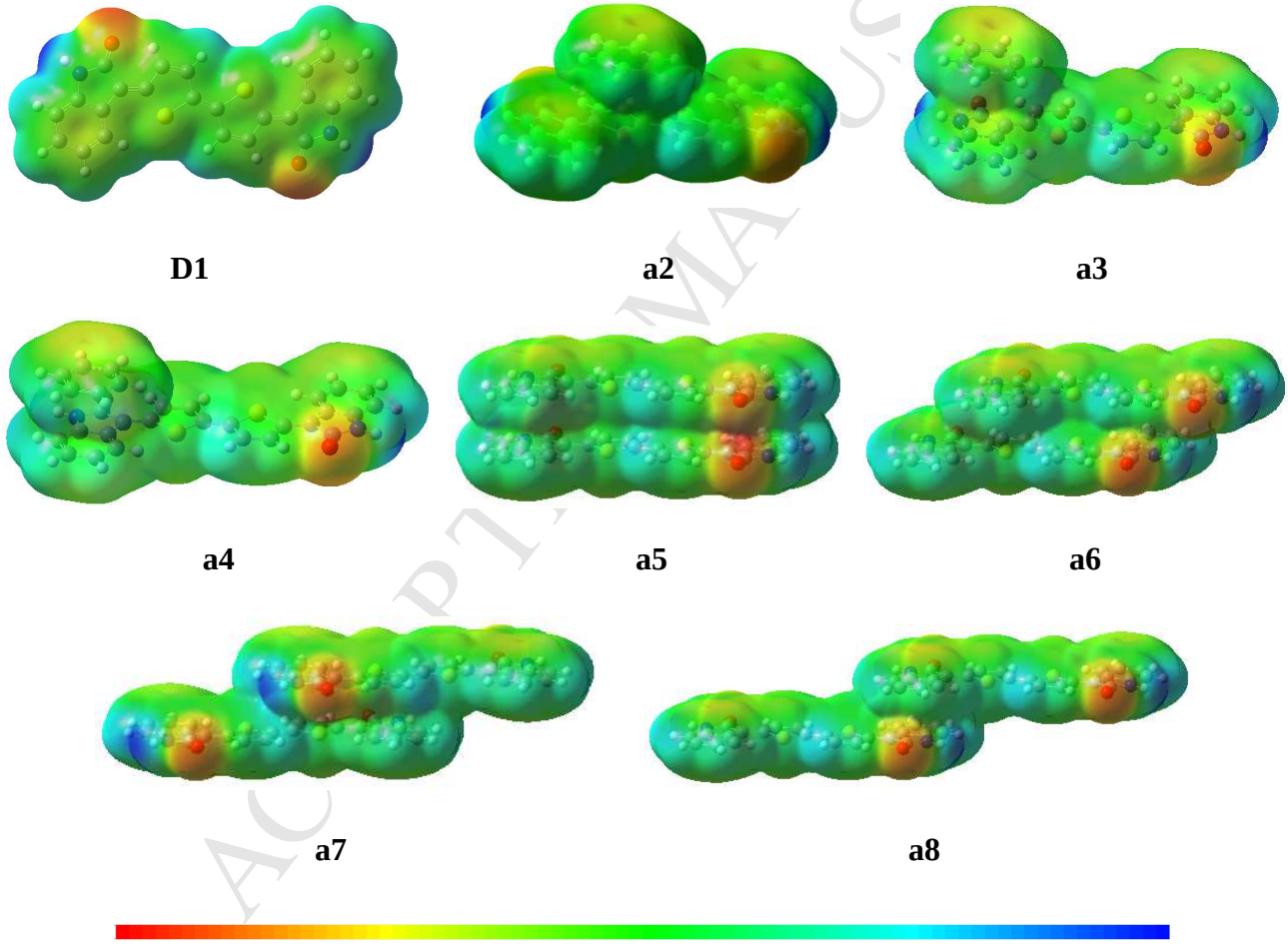

Note: Red indicates the highest electronegativity; blue indicates the highest electropositivity.

Fig. 10. Electrostatic potential energy diagrams of **D1** (front view) and **a2**-**a8** (side view).

The effect of halogen atoms on the interaction energy was also studied by comparing dyes **D1**-**D3**. For indophenine-benzene interactions, initial interaction models for **D2** and **D3** were obtained by adopting the **a3** configuration as shown in **Fig. S3**, though little difference was found (**Fig. S4**). Since the F/Cl substituted sites were much closer to the ring overlapping center in the **a4** configuration than that of **a2** or **a3**, the configurations of **D2** and **D3** were rebuilt by adopting the **a4** configurations of **D1** (**Fig. 11**). As shown in **Fig. 12**, the lowest interaction energy values for **b1** (-26.28 kJ/mol) and **c1** (-28.77 kJ/mol) configurations were lower than the **a4** configuration (-22.74 kJ/mol). For indophenine-indophenine interactions, models were constructed similarly to the **a6** configuration. The lowest interaction energy values were -121.94 kJ/mol for the **b2** configuration and -126.36 kJ/mol for the **c2** configuration. This suggests that the introduction of fluorine or chlorine atoms effectively enhances the intermolecular interaction. While the relatively large interaction energy for halogen atom substituted indophenine dyes could help to obtain better dye anti-thermomigration, dye-dye forces that are large also promote dimer or oligomer formation. Thus, the difficulty to form single dye molecules resulted in experimentally low color acquisition for F/Cl atom substituted dyes.

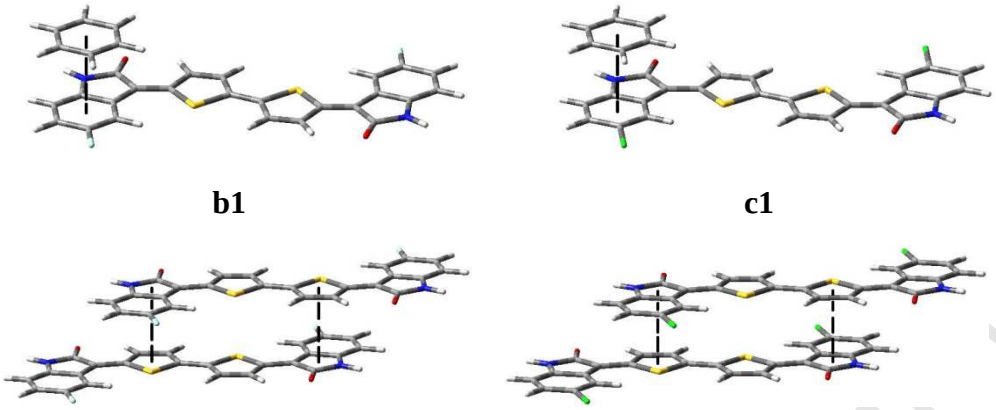

Fig. 11. Molecular interaction energy models for **D2** and **D3**.

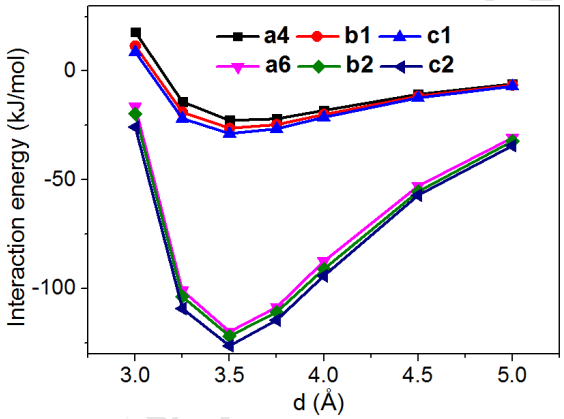

Fig. 12. Indophenine-benzene and indophenine-indophenine interaction energy for **D1**-**D3**.

4. Conclusions

In summary, a series of indophenine dyes **D1**-**D6** that contain *N*-ethyl groups or F/Cl atoms have been facilely synthesized through the "indophenine reaction" with isatin derivatives as starting materials. Although these indophenine dyes showed very low solubility in common organic solvents, we have revealed a promising application that provides blue shades on polyester fabrics.

The large and planar indophenine backbone produces both strong dye-dye and dye-fiber forces. On one hand, this is beneficial for preventing dye molecules from leaving dyed fabrics, leading to

improved washing, rubbing, and sublimation fastness. On the other hand, the lower dyeing rate of indophenine dyes compared to that of conventional azo/anthraquinone dyes results in higher dyeing temperature necessary to form single dye molecules in order to facilitate the dyeing process.

Study of the substituent effect demonstrated that *N*-ethyl groups could improve the dye uptake, while F/Cl atoms would inhibit the dyeing performance. As a result, **D4** with only two *N*-ethyl groups showed the best overall dyeing performance. DFT calculations demonstrated that there exists both a large indophenine-benzene interaction energy and a indophenine-indophenine interaction energy for indophenine dyes. F/Cl atom substituted indophenine dyes were found to have larger interaction energies, leading to better anti-thermomigration properties. This study provides a preliminary suggestion for the rational design of new disperse dyes based on indophenine structure. Further study of improving dyeing performance by extension of this family of indophenine dyes is now on going in our group.

Acknowledgement

This work was supported by the National Natural Science Foundation of China (No. 21808210, 51673176), Public Welfare Technology Research Project of Zhejiang Province (LGG18B060003), Zhejiang Provincial Natural Science Foundation of China (LY16B060006), Zhejiang Provincial Top Key Academic Discipline of Chemical Engineering and Technology of Zhejiang Sci-Tech University (CETT2016002) and Science Foundation of Zhejiang Sci-Tech University (ZSTU) under Grant No. 16012087-Y.

Appendix A. Supplementary data

For supplementary data related to this article, see supplementary information.

References

[1] Qian HF, Song XY. The structure of azo disperse dyes and its distribution on polyurethane fiber blend with polyester, or polyamide fiber. Dyes Pigm 2007;74:672-6.

[2] Suwanruji P, Chuaybamrung L, Suesat J. Study of the removal of a disperse dye stain from a polyester/elastane blend. Color Technol 2012;128:103-7.

[3] Sokolowaka J, Podsiadly R, Sochocka E. Synthesis and properties of some disazo disperse dyes derivatives of 2-amino-6-phenylazothiazole and 2-amino-6-(4'-nitro)-phenylazobenzothiazole. Dyes Pigm 2007;72(2):223-7.

[4] Patel DM, Patel TS, Dixit BC. Synthesis, characterization and dyeing performance of new bisazoebisazomethine disperse dyes. J Saudi Chem Soc 2013;17(2):203-9.

[5] Kim SD, Kim MJ, Lee BS, Lee KS. Effects of thermomigration on the washfastness of disperse dyes having different molecular size. Fibers Polym 2004;5(1):39-43.

[6] Feng GF, Qian HF, Bai G, Liu YC, Hu LL. Synthesis, characterization, and application of diester/diurethane tethered azo disperse dyes: A new strategy to improve dyes' fastness properties. Dyes Pigm 2016;129:54-9.

[7] Qian HF, Feng GF, Bai G, Liu YC, Hu LL. A contrastive study of adsorption behaviors on polyurethane fiber with diester/diurethane tethered and non-tethered azo disperse dyes. Dyes Pigm 2017;145:301-6.

[8] Joshi M, Jauhari S, Desai KR. Polyurethanes as polymerizable dyes for hydrophobic polyester fabric. Res Chem Intermed 2012;38(9):2137-48.

[9] Singh A, Choi R, Choi B, Koh J. Synthesis and properties of some novel pyrazolone-based heterocyclic azo disperse dyes containing a fluorosulfonyl group. Dyes Pigm 2012;95:580-6.

[10] Dodangeh M, Yousefi N, Mohammadian M. Synthesis and functionalization of polyamidoamine dendrimers with thiazol derivatives to prepare novel disperse dyes and their application on polyethylene terephthalate (PET). Dyes Pigm 2015;116:20-6.

[11] Ameuru US, Yakubu MK, Bello KA, Nkeonye PO, Halimehjani. Synthesis of disperse dyes derived from 4-amino-*N*-decyl-1,8-naphthalimide and their dyeing properties on polyester fabrics. Dyes Pigm 2018;157:190-7.

[12] Zhan YZ, Zhao X, Wang W. Theoretical study of the interaction energy of benzodifuranone dye molecule rings. Color Technol 2016;133:50-6.

[13] Zhan YZ, Zhao X, Wang W. Synthesis of phthalimide disperse dyes and study on the interaction energy. Dyes Pigm 2017;146:240-50.

[14] Zhan YZ, Zhao X, Wang BJ, Wang W. Computational modeling of the influence of substituent effects on phthalimidylazo disperse dye hydrolysis and interaction energy. Color Technol 2017;134:24-32.

[15] Casado J, Rocio PO, Juan TN. Quinoidal oligothiophenes: new properties behind an unconventional electronic structure. Chem Soc Rev 2012;41:5672-86.

[16] Burrezo PM, Zafra JL., Navarrete JTL., Casado, J. Quinoidal/aromatic transformations in π-conjugated oligomers: vibrational raman studies on the limits of rupture for π-bonds. Angew Chem Int Ed 2017; 56:2250-9.

[17] Colella L, Brambilla L, Nardone V, Bertarelli C. Outside rules inside: the role of electron-active substituents in thiophene-based heterophenoquinones. Phys Chem Chem Phys 2015;17:10426-37.

[18] Jiang H, Oniwa K, Xu ZQ, Bao M, Yamamoto Y, Jin TN. Synthesis and properties of dicyanomethylene-endcapped thienopyrrole-based quinoidal *S*,*N*-heteroacenes. Bull Chem Soc Jpn 2017;90(7):789-97.

[19] Jiang H, Zhang L, Cai JF, Ren JH, Cui ZH, Chen WG. Quinoidal bithiophene as disperse dye: Substituent effect on dyeing performance. Dyes Pigm 2018;151:363-71.

[20] Tormos GV, Belmore KA, Cava MP. The indophenine reaction revisited. Properties of a soluble dialkyl derivative. J Am Chem Soc 1993;115:11512-5.

[21] Hwang H, Khim D, Yun JM, Jung E, Jang SY, Jang YH, et al. Quinoidal molecules as a new class of ambipolar semiconductor originating from amphoteric redox behavior. Adv Funct Mater 2015;25:1146-56.

[22] Deng YF, Sun B, He YH, Quinn J, Guo C, Li Y. Thiophene-*S*,*S*-dioxidized indophenine: a quinoidal-type building block with high electron affinity for constructing n-type polymer semiconductors with narrow band gaps. Angew Chem Int Ed 2016;55:3459-62.

[23] Zheng J, Huang F, Li YJ, Xu TW, Xu H, Jia JH, et al. The aggregation-induced emission enhancement properties of BF_2 complex isatin-phenylhydrazone: Synthesis and fluorescence characteristics. Dyes Pigm 2015;113:502-9.

[24] Damgaard M, Al-Khawaja A, Vogensen SB, Jurik A, Sijm M, Lie MEK, et al. Identification of the first highly subtype-selective inhibitor of human GABA transporter GAT3. ACS Chem Neurosci 2015;6:1591-9.

[25] Frisch MJ, Trucks GW, Schlegel HB, Scuseria GE, Robb MA, Cheeseman JR, et al. Gaussian 09, Revision E.01, Wallingford CT: Gaussian Inc.; 2009.

[26] Takahashi T, Matsuoka K, Takimiya K, Otsubo T, Aso Y. Extensive quinoidal oligothiophenes with dicyanomethylene groups at terminal positions as highly amphoteric redox molecules. J Am Chem Soc 2005;127:8928-9.

Highlights

- A series of indophenine dyes containing *N*-ethyl groups or F/Cl atoms were synthesized.
- The synthesized blue indophenine dyes could dye polyester fabric with excellent wet fastness.
- The quinoidal planarity of indophenine molecule provides large intermolecular interaction energy.
- *N*-ethyl groups favor the dyeing process, while fluorine or chlorine atoms lower the color acquisition.